Cluster formation mechanisms of titanium dioxide during combustion synthesis: observation with an APi-TOF

Jiaxi Fang[1,#], Yang Wang[1,#], Juha Kangasluoma[2], Michel Attoui[2,3], Heikki Junninen[2], Markku Kulmala[2], Tuukka Petäjä[2], Pratim Biswas[1*]

[1]Aerosol and Air Quality Research Laboratory
Department of Energy, Environmental and Chemical Engineering
Washington University in St. Louis
St. Louis, MO-63130

[2] Department of Physical Sciences,

University of Helsinki, P.O. Box 64, Helsinki, 00014, Finland

[3] LISA Université paris Est, Diderot, Créteil, 7583, France

Submitted to:

Aerosol Science and Technology

# These two authors contributed equally to this work.

* To whom correspondence should be addressed:

Tel: +1-314-935-5548; Fax: +1-314-935-5464

E-mail address: pbiswas@wustl.edu

Abstract

Few studies reported the formation of Ti-containing clusters in the initial stages of TiO_2 flame synthesis. The conversion from synthesis precursor to TiO_2 monomers was commonly assumed to take place through global reaction such as thermal decomposition and/or hydrolysis at high temperatures. More recent studies have been able to identify stable intermediates of Ti-containing monomers, most commonly $Ti(OH)_4$, as the final step before the formation of TiO_2. However, no larger Ti-containing cluster formation mechanisms or interactions between these monomers have been tracked. To investigate cluster formation pathways of TiO_2 during flame synthesis, Charged clusters were measured in an atmospheric pressure interface time-of-flight (APi-TOF) mass spectrometer. TiO_2 nanoparticles were synthesized by adding titanium tetraisopropoxide (TTIP) precursor to a premixed $CH_4/O_2/N_2$ flat flame aerosol reactor. Pure TiO_2 clusters were not detected by the APi-TOF. Results from measured mass spectra and mass defect plots show that for positively charged clusters, the abstraction of CH_2 groups occurs simultaneously with the clustering of larger intermediate organometallic species. For negatively charged clusters, NO_x formation pathways in the flame may play a role during the initial stages of TiO_2 formation, since a lot of Ti-containing clusters were attached with nitrate-related species. These research findings provide insights on quantum dot synthesis and molecular doping where rapid dilution of the flame synthesized nanoparticles is needed to better control the particle size and chemical composition. The possible influences of and potential artifacts brought by the dilution system on observing the incipient particle formation in flames were also discussed.

1. Introduction

The mechanisms of initial particle (clusters) growth from gaseous precursors is not well understood. These mechanisms are especially important for the combustion synthesis of nanoparticles such as TiO_2, which is most commonly manufactured through this route for use as a photocatalyst, semiconductor, or pigment (Swihart 2003; Hu et al. 2016; Li et al. 2016; Pratsinis 1998; Liu et al. 2015). Although significant work has focused the nucleation mechanisms of particles in the atmosphere, aerosol nucleation and growth in flames that occurs at high temperatures (up to 2400K) at extremely high rates of production have not been studied extensively. Early stage mechanisms are critical in accurately modeling overall particle growth, especially for multicomponent systems. It is well understood that particle growth beyond 2 nm in flames occurs through collision, condensation, and sintering processes. Applications of combustion synthesis to novel materials, such as battery anodes, catalysts, and solar cells have been difficult to scale up since particle growth cannot be modeled accurately from first principles and must rely on empirical approaches. In the case of combustion synthesis of metal oxides, calculations based on classical nucleation theory predict that the critical monomer size is a single monomer of TiO_2 (Ulrich 1971). The validity of this assumption has yet to be experimentally proven.

Various approaches have been developed to track particle formation and growth in flames. For example, laser-induced breakdown spectroscopy (LIBS) is a non-invasive method for *in situ* diagnostics both for pristine (Zhang et al. 2013) and doped metal oxide (Liu et al. 2016) nanomaterials in flames which can differentiate between particle and gas phase atoms (Ren et al. 2015). Laser Induced Fluorescence (LIF) spectroscopy has been successfully applied to

premixed flames to study the synthesis of iron oxide-silica composites and compared to aerosol growth models (Biswas et al. 1997; McMillin et al. 1996). However, these techniques do not provide sufficient detail regarding the chemistry of particle formation. Molecular beam mass spectrometry (MBMS) is the most widely used direct sampling technique for mapping the chemistry and kinetics of hydrocarbon combustion (Hansen et al. 2009) and oxide formation in hydrogen flames (Kluge et al. 2016; Shmakov et al. 2013), but this technique typically requires low-pressure conditions to conduct combustion, and is unable to provide size resolved chemistry or track larger cluster formation mechanisms.

Electrical mobility measurements, a well-established method of measuring particle size distributions, have allowed detailed measurements of particle growth and coagulation. However, resolution limitations and diffusion losses below 2 nm make the technique unsuitable for tracking smaller clusters (Wang et al. 2014). Significant advances in high resolution differential mobility analyzers (HRDMAs) have allowed measuring and tracking cluster growth during the combustion synthesis of TiO_2 for the first time (Fang et al. 2014). HRDMAs have been applied to studying mass-mobility relationships of particles below 3 nm experimentally (Larriba et al. 2011) along with direct comparisons to computational predictions of electrical mobility (Larriba and Hogan Jr 2013). These techniques can now provide insights into cluster formation mechanisms in flames (Wang et al. 2017a; 2017b; 2017c). As pointed out by a recent study conducted with these instruments, the fraction of natively charged particles in total particles in the size range below 3 nm may be extremely high (Wang et al. 2017b). Advancements in atmospheric pressure interface time of flight mass spectrometers (APi-TOF) have allowed for high resolution identification and detection of ions directly at atmospheric pressure (Junninen et

al. 2010), with applications in areas such as the study of atmospheric nucleation events (Kulmala et al. 2013).

This paper is focused on understanding the initial stages of TiO_2 particle formation in a premixed flat flame, as measured by an APi-TOF. Measurements are taken through a Venturi dilution probe which draws a sample of charged clusters into the APi-TOF at a dilution ratio of 180. Probable pathways and cluster formation mechanisms are presented for the first time on the initial stages of particle formation in the combustion synthesis of TiO_2.

2. Material and Methods

2.1 Experimental Setup

[Figure 1 here]

A premixed flat flame aerosol reactor (FLAR) generated clusters of TiO_2 (Figure 1). Details of the FLAR are described in previous work (Fang et al. 2014). Briefly, a radially symmetric flat flame was stabilized over a 1.91 cm diameter honeycomb burner head inside a concentric 2.54 cm diameter tube which provided a sheath flow of N_2 gas (>99.95%, Linde AG). Gas flow rates for methane (>99.95%, Linde AG), oxygen (>99.95%, Linde AG), nitrogen carrier gas and TTIP precursor (Sigma Aldrich Inc., >97%) were metered by mass flow controllers (MKS Instruments). A stainless-steel feed tube from the precursor bubbler was heated to prevent precursor wall condensation. A sealed glass bubbler (MDC Vacuum Products, LLC) supplied TTIP precursor to the premixed flame using nitrogen as the carrier gas. The feed rate was calculated based on relationships from (Siefering and Griffin 1990). The precursor molar feed rate ranged from 0.07 mmol/hr to 0.22 mmol/hr (2.8 to 8.8 ppm). Flow conditions for the FLAR

are listed in Table 1. The flame equivalence ratio was 0.7. All of the gases were premixed prior to entering the burner head creating a stable flame sheet at the burner-head.

[Table 1 here]

To quench further chemical reactions and particle growth in the flame, a venture dilution probe using nitrogen as a dilution gas at a dilution ratio of 180:1 (dilution flow rate : sample flow rate) was used. Flame-generated clusters were sampled 5 mm above the burner head. The dilution flow rate was maintained at 25 lpm by a mass flow controller (MKS Instruments). The temperature profile above the burner without the insertion of the dilution probe can be found in Fig. S1. With the addition of the sampling probe, the local temperature will be inevitably reduced. Existing studies showed that a difference of 500 K was expected due to the perturbation of inserting the dilution probe (Zhao et al. 2003). Due to this temperature decrease, combustion and reaction of TTIP may be interfered. Natively charged flame ions and clusters were injected into an APi-TOF mass spectrometer (Tofwerk AG, Thun) where the mass to charge ratio (*m/z*) was measured in the unit of Thomson (Th). The inlet flow rate to the entrance of the APi-TOF mass spectrometer was 0.81 lpm and the excess flow was exhausted. The APi-TOF was operated without additional ionization sources, so only natively charged clusters were sampled into the mass analyzer. This system is capable of measuring both positive and negative ions with a resolution of 3000 Th/Th (M/ΔM), a mass accuracy better than 20 ppm, and a detection range of up to 2500 Th. Further details of this instrument can be found in previous publications (Junninen et al. 2010). The confirmation of molecular compositions considers both the highly accurate mass and isotope distribution of a probable species. Speculated chemical formulae were assumed to contain C, H, O, N, S, and Ti. By limiting the maximum and

minimum number of atoms (50 and 0), probable chemical compositions and regarding differences in ppm were calculated. The speculated chemical compositions shall have low mass differences compared to the measured mass values, possess appropriate isotope distributions, and be chemically stable. Before the measurement of flame-generated charged clusters, calibration of measured mass was performed using NO_3^- (61.9878 Th), HNO_3 NO_3^- (124.9835 Th) and $(HNO_3)_2$ $(NO_3)_3^-$ (187.9791 Th) for negative clusters. Positively charged clusters were calibrated using NH_4^+ (18.0344 Th), $((CH_3)_2CO)H^+$ (59.0497 Th) and $((CH_3)_2CO)_2H^+$ (117.0916 Th). These negative or positive ions were either generated from a radioactive neutralizer (Kr-85, Model 3077, TSI Inc.) or by feeding acetone vapors through the radioactive neutralizer. The switch of the detection polarity was done by altering the acquisition methods in the software (TofDaq, TOFWERK AG, Thun). The APi-TOF has the same characteristics, for example, resolution and sensitivity, for negatively and positively charged clusters. The data analysis was conducted with tofTools, a Matlab software developed by Junninen et al. (2010) The particle loss in the system took place predominantly in the APi-TOF, which was reported to have a transmission efficiency of 0.1 to 0.5% (Junninen et al. 2010). It should be noted that sampling in flames with a probe will inevitably alter a sample. Although it has been carefully calibrated, the dilution sampler used in this study may not be sufficient to quench all reactions and particle dynamics. Regarding influences of and potential artifacts brought by the dilution sampling system are discussed in section 3.4.

2.2 Experimental plan

[Table 2 here]

Table 2 presents the experimental plan. Four different tests were performed, starting with the measurement of background ions in the methane-air flat flame without any precursor (Test 1). Following Test 1, TTIP precursor was added to the flat flame to measure Ti-containing clusters for both positively charged clusters (Test 2) and negatively charged clusters (Test 3). Finally, the effect of feed rate was studied by adjusting the feed rate of the precursor (Test 4).

2.3 Reaction mechanisms of TiO_2 in flames

Particle formation of TiO_2 from the decomposition of TTIP is assumed to occur through thermal decomposition and/or hydrolysis at high temperatures. Although TTIP is a commonly used precursor for the study of TiO_2 combustion synthesis, detailed chemical mechanisms of conversion have only recently been explored (Shmakov et al. 2013). The kinetics of thermal decomposition of TTIP have been measured by(Okuyama et al. 1990) by assuming the following first order reaction mechanism:

$$Ti\ (OC_3H_7)_4 \rightarrow TiO_2 + 2H_2O + 4C_3H_6 \quad (1)$$

By measuring sub 2nm cluster size distributions with a Half-Mini DMA, revised first order reaction rates were derived assuming the same mechanism (Wang et al. 2015). At low temperatures (< 400 ^oC), the thermal decomposition of TTIP (Ahn et al. 2003) may also take place through

$$Ti\ (OC_3H_7)_4 \rightarrow TiO_2 + 2C_3H_7OH + 2C_3H_6 \quad (2)$$

Finally, water in flames results in rapid hydrolysis of TTIP. Hydrolysis has been recognized to be the dominant pathway of TTIP conversion to TiO_2 (Tsantilis et al. 2002):

$$Ti\ (OC_3H_7)_4 + 2H_2O \rightarrow TiO_2 + 4C_3H_7OH \quad (3)$$

Molecular beam mass spectrometry (MBMS) in a hydrogen flat flame with TTIP precursor addition has provided a more detailed conversion mechanism for the hydrolysis of TTIP to TiO_2. $Ti(OH)_4$ has been shown to be the most stable intermediate byproduct of hydrolysis (Shmakov et al. 2013). It should be noted that although these reactions are written in global reaction formulae, the they were not single-step reactions. Detailed reaction pathways of titanium isopropoxide has been simulated with *ab initio* calculations to evaluate the rate constants of separate steps, suggesting that the thermal decomposition reactions of TTIP and isopropanol were similar (Buerger et al. 2005, 2017). The flux analysis done by Buerger et al. (2017) showed that the sequential release of C_3H_6 groups was the major reaction pathway of TTIP, and $Ti(OH)_4$ was the most stable product before its final conversion to TiO_2.

3. Results and discussion

3.1 Background ions measured in methane-air premixed combustion

[Figure 2 here]

To study background ions in the flame, positively and negatively charged clusters were measured in a premixed fuel lean methane-air flat flame without any precursor addition. The results are displayed in Figure 2. Previous studies of ions in flames have focused on lower molecular weight species which have undergone further ionization steps (e.g., electron ionization or vacuum ultraviolet ionization) (Fialkov 1997; Jones and Hayhurst 2016). Recently, HR-DMAs have been used to measure the mobility spectra for natively charged flame ions in a fuel-lean methane-air flat flame, however further steps need to be taken to measure the exact mass of ions (Fang et al. 2014). The mass spectra in Figure 2 represent natively charged clusters sampled from the flame. The peaks from the positively charged mass spectrum are mostly organic

radicals commonly measured during methane-air combustion, for example, the most prominent peak was measured with an *m/z* of 124 with probable molecular composition of $C_4H_{14}O_3N^+$(*m/z*=124.0974 Th). Because of the high abundance of hydrogen atoms in this formula, this molecule may be a nitrogen-containing hydrocarbon clustered with one or several water molecules. However, it is difficult to speculate the molecule structures based on the limited information on molecular mass. In the case of negatively charged species, the ions were identified as nitrate radicals and nitric acid clusters of NO_3^-(*m/z*= 61.9878 Th), HNO_3 NO_3^- (*m/z*=124.9835 Th), and $(HNO_3)_2$ $(NO_3)_3^-$ (187.9791 Th), which might be generated through the combustion pathways of NO_x formation. NO_x is long established as a combustion pollutant playing an important role in emissions from hydrocarbon flames. Three main pathways of combustion induced formation of NO_x include fuel-NO_x, thermal NO_x and prompt NO_x (Nicol et al. 1995). Since the fuel and precursor do not contain any nitrogen species and the flame temperature is on the order of 1300-1800K, prompt NO_x is likely the primary mechanism of NO_x formation from collisions of N_2 gas molecules with the high concentration of radicals in the flame. Similarly, significant concentrations of NO_x has also been detected in previous studies for premixed $CH_4/O_2/N_2$ flames (Debrou et al. 1980). The presence of diverse ion species in flames complicates the particle formation in early stages, as previous work studying particle formation and growth in flames do not account for electrostatic interactions among ions and particles. Thus, understanding the role of various charging mechanisms and their interaction with particle coagulation will be important for understanding and modeling clustering interactions in flames (Jiang et al. 2007; Wang et al. 2017c; Nie et al. 2017).

3.2 Titanium dioxide particle formation during combustion synthesis

[Figure 3 here]

[Figure 4 here]

The addition of TTIP precursor in the flame resulted in the generation of charged titanium species providing insight into the initial stages of particle formation for TiO_2 during combustion synthesis. Figure 3 displays the mass spectra for negatively charged clusters, while Figure 4 displays the positive ion spectra. The feed rates of 0.07, 0.15, and 0.22 mmol/hr correspond to TTIP concentrations of 2.8, 6.0, and 8.8 ppm. Ti contains five naturally occurring stable isotopes: $^{45.9526}$Ti (10.8%), $^{46.9518}$Ti (9.9%), $^{47.9480}$Ti (73.8%), $^{48.9479}$Ti (7.5%), $^{49.9448}$Ti (7.3%), allowing for the identification of Ti-containing clusters through this isotopic pattern. For the negative ion mass spectra, distinct monomer ions with Ti could be identified as TiO_2 $(NO_3)_3$ at *m/z* of 266 Th. Additional peaks of TiO_2 with multiple NO_3 species attached were also present in the mass spectra, while Ti species with varying levels of oxidation were also measured in the form of $Ti_nO_xN_y$. Peak assignments for negatively charged Ti-containing clusters, listed in Table 3, are an indication that flame ions participate in the conversion from TTIP to TiO_2, with NO_x playing an important role. Furthermore, a previous study using an enhanced particle counter coupled with a charged particle remover indicated that the charge fraction of incipient particles generated from flame synthesis was high (may be as high as 80% when TTIP concentration was below 8.8 ppm) (Wang et al. 2017b). This high charge fraction further signified the influence of ion environment during particle synthesis. Recent studies using plasma-assisted combustion and electric field-assisted combustion also utilized the electrical properties of combustion (Park et al. 2016; Xiong et al. 2017a; Xiong et al. 2017b; Ren et al. 2017). We should note that it is also possible that the attachment of nitrate species may be completed in the sampling system, where the rapid cooling altered the equilibrium of reactions. However, the obtained knowledge can be

applied to molecular doping and the synthesis of quantum dots during combustion, where rapid dilution is needed in these scenarios.

[Table 3 here]

For positively charged clusters, protonated clusters in the form of $Ti(OH)_4H^+$ and $Ti(OH)_3H^+$ were identified in addition to $TiO(OH)_4^+$ (Figure 4). These were the most prominent monomer Ti- containing species in the positive mass spectra, which is in agreement with previous literature, showing titanium hydroxide to be the most stable intermediate from TTIP hydrolysis (Buerger et al. 2015; Shmakov et al. 2013). Larger peaks could not be identified due to significant isotope overlap and multiple possible molecular compositions at higher masses. The peak assignments contained many possible organic species, thus complicating the positive mass spectra and indicating the incomplete decomposition of TTIP. Furthermore, these intermediates may have interacted with organic radicals and flame ions. Previous studies on flame ions have concluded that chemical ionization mechanisms are important in hydrocarbon flames near the flame sheet and many unburnt hydrocarbons can also contribute to ionization and charging mechanisms (Fialkov 1997).

Beyond 300 Th, periodic humps with distinct cluster isotope patterns become increasingly prevalent with increasing precursor concentration (Figure 4). Each hump was a combination of isotope distributions of Ti-containing clusters with close atomic mass values. In this size range, isotopic patterns of titanium clusters ions begin to overlap, making the spectra complicated to interpret. Previous studies using TOF mass analyzers studying pure TiO_2 nanoparticles have experienced similar issues with peak assignments (Guan et al. 2007). Cluster peaks can be

grouped together by their isotope patterns. Each cluster is separated by 14 Th, indicating the abstraction of CH_2 groups. The separation of each hump was approximately 140 Th, representing the abstraction of CH_2 groups by ten times during the removal of organic groups in TTIP molecules. This phenomenon can be seen more clearly from the mass defect plot shown in the next section. Since there are twelve CH_2 groups in a TTIP molecule, this band of 140 Th suggested that not all of the CH_2 groups were removed from the precursor molecule, or the precursor molecules lose several CH_2 groups to become positively charged. Each hump peaked in the middle, indicating clusters with moderate number of CH_2 groups were more stable. These periodic peak patterns also show that intermediates from TTIP decomposition may polymerize or aggregate into larger clusters prior to conversion to pure TiO_2. In Figure 4c, beyond 300 Th, these patterns resemble organic cluster formation as observed in previous atmospheric nucleation studies. Organic molecule attachment on the larger Ti-containing clusters further complicates the assignment of mass spectral peaks. There are two potential sources of such organics: methane combustion may generate a high concentration of organic ions that attach onto TTIP clusters, while TTIP is an organometallic precursor with 4 propyl groups which can be charged through chemical ionization in the flame. The attachment of organic ions on Ti-containing clusters can be evaluated through the comparison of characteristic charging time and transport time of flame-generated charged and neutral species. Existing measurements of ion concentrations (n) in flames report values in the order to 10^{17} /m^3 (Fialkov 1997), while the ion attachment coefficient (k) on particles below 2 nm at temperatures above 1000 K was in the order of 10^{-14} m^3/s (Wang et al., 2017c). These parameters result in a characteristic charging time ($2/nk$) in the order of 2 ms. The particle residence time in the first 5 mm from the burner to the sampling probe was approximately 1.5 ms (by considering the thermal expansion and by

assuming an average temperature of 1600 K). The similar magnitude of these two time scales indicate that the detected large organics may be a result of ion attachment on Ti-containing precursor clusters. Based on the ratios of isotopic peaks to the main peak, we can conclude that the clusters contain multiple titanium atoms. Apart from the more prominent band pattern at higher m/z with the increased TTIP feed rate, stronger signals at 438, 450, and 462 Th were also detected. Based on the high-resolution mass differences among these clusters, these three clusters may have the formulae of $C_xH_yO_zN_aTi_b$, $C_{x+2}H_{y+4}O_{z-1}N_aTi_b$, and $C_{x+2}H_{y+4}O_{z-1}N_{a+2}Ti_b$. Due to isotope peak overlap and the multiple combinations of potential compounds at high mass ranges, exact peak assignments could not be performed, thus mass defect techniques were used to provide further insight into the mass spectra.

3.3 Mass defect plots

[Figure 5 here]

Mass defect plots from the positive and negative mass spectra were constructed from Figure 3b and 4c to provide another visual basis for analyzing the complex mass spectrum (Figure 5). Here peaks with a signal higher than 0.25 counts per second (cps) were each assigned a calculated mass defect and plotted with the mass defect on the y-axis and isotope mass on the x-axis. A mass defect is defined as the difference between a compound's exact mass and nominal mass. For example, the isotopes of Ti have mass defect values of -0.0474, -0.0482, -0.0520, -0.0521, and -0.0552 Th for $^{45.9526}$Ti, $^{46.9518}$Ti, $^{47.9480}$Ti, $^{48.9479}$Ti, $^{49.9448}$Ti, respectively, resulting in a spread of data points with a negative slope in the mass defect plot. Plotting the mass defect allows for visualization of complex mass spectra and has been successfully applied towards analyzing mass spectra from crude oil (Hughey et al. 2001) and atmospheric organic molecules (Schobesberger

et al. 2013), where similar repeating peak patterns have been observed. In the case of combustion synthesis of TTIP, the mass defect plot spans from positive to negative mass defect ranges, which helps identify the class of compounds in the spectrum. Positive mass defects indicate the presence of organics (e.g. CH_2 has a mass defect of +0.0156), and negative mass defects indicate oxidized species of titanium clusters (e.g., TiO_2 has a mass defect of -0.062).

Figure 5a displays several distinct bands for positively charged clusters (labeled as "Cluster X"). In each band, there are clusters lining up with a constant negative slope, as shown by the dashed lines. This is caused by the spread of Ti isotopes in a same molecule as discussed in the above. The width of the spread also becomes larger at higher m/z values, resulting from the existence of multiple Ti atoms in the larger clusters. The gap between each cluster in each band is 14.016 Th, representing the abstraction of CH_2 groups in each band. The abstraction of CH_2 groups happened 10 times in a precursor molecule, since the length of each band is approximately 140 Th. Based on this result, the left end of each band corresponds to a Ti-containing cluster with the fewest hydrocarbon groups. The mass defect values of the left end in each band become more negative, resulting from the significant mass defect through the addition of a Ti atom (-0.047 Th). However, the mass difference between the left ends of each band was approximately 150 Th, not the value corresponding to Ti or TiO_2. This result suggested that the primary "building block" during the clustering of incipient particles contain species other than Ti and O, for example, hydrocarbon and nitrogen. Above the Cluster 2 in Figure 5a, there is another band of clusters showing a similar slope to Cluster 1. This band show that Cluster 1 may be attached with multiple propyl groups, so that CH_2 abstraction started from clusters with higher molecular masses. It should be noted that at higher masses, the mass defect plot distorts to progressively

more negative slopes, indicating that the TOF calibration has drifted in this mass range. This may be caused by the fact that the calibration was conducted with species of smaller m/z values (< 200 Th). Further studies will require more sophisticated calibration procedures to ensure accurate peak identification at higher masses.

For the negative mass defect plot (Figure 5b), the spectrum does not have the same distinct groupings of clusters, but the overall negative slope indicates strong clustering interactions of $(TiO_2)_x (NO_3)_y$. Identifiable peaks in Figure 4 are mostly a class of negatively charged $Ti_nO_xN_y$ clusters. Due to the different possible oxidation states of Ti, the assignment of oxygens to either Ti or N is ambiguous. However, the band structure spacing as seen in the positive mass defect plot with spacing's of 16 Th also indicate the addition of O to $Ti_nO_xN_y$ complexes, providing further evidence for strong clustering interactions between NO_x and Ti species. A dashed line with a slight upward slope also highlights that OH^- radical-driven interactions participated in the growth of Ti-containing clusters. Further studies are needed to fully understand the contribution of chemi-ionization pathways during combustion synthesis.

Based on the data presented in Figures 3-5, we can see that collisional growth of TiO_2 molecular ion clusters at the initial stages of particle formation may not be a suitable assumption to capture the growth mechanisms. Previous studies have concluded that $Ti(OH)_4$ is the most thermodynamically stable monomer. Based on positive mass spectra similar conclusions can be drawn since $Ti(OH)_4$ and $TiO(OH)_4$ had the highest intensities. Negative mass spectra revealed the presence of $Ti_nO_xN_y$ species demonstrating the importance of chemical ionization. For example, single monomer ions of Ti contained varying number of O atoms. Even for dimers and

trimers of Ti, the ratio of Ti to O varied. Nevertheless, many other stable intermediates were also measured, and clusters containing more than a single Ti atom were detected in significant concentrations. Thus there is a need to further understand how these larger clusters form and how they affect downstream pathways. Previous approaches to aerosol modeling neglected the role of chemistry and intermediate species during cluster growth, where it was assumed that discrete clusters had a uniform chemical composition. More accurate models should aim to couple chemical reactions beyond monomer formation, which may take place after the initial precursor decomposition step as larger clusters begin to form. Intermediate species may continue to form during cluster growth, thus future work should aim to understand how intermediate species may interact and at what point physical aerosol growth processes take over

3.4 Discussion on the dilution sampling system

The sampling of incipient particles from high temperatures is challenging, because the dilution probe should sufficiently quench all particle growth dynamics and gas-phase reactions during the particle transport in the sampling line. On the other hand, the perturbation to flames caused by the insertion of the dilution probe should also be minimized. Concerns may be raised regarding the validity of the measurement, especially in such a minuscule size range, where the particles may be very unstable.

As shown in Fig. S1, the temperature at the sampling location (5 mm above the burner) was approximately 1800 K without the interference of the sampling probe. With the addition of the sampling probe, the local temperature will be reduced by approximately 500 K according to previous studies (Zhao et al. 2003). Due to this temperature decrease, combustion and reaction

of TTIP may be interfered. The characteristic reaction time of TTIP can be evaluated using the one-step reaction rates of TTIP. The first-order reaction rate of TTIP thermal decomposition is $k_g = 3.96\times10^5 \exp(-8480/T)$. The characteristic reaction time is then calculated by $\tau_{rxn} = 1/k_g$. Based on the calculation, the reaction time scale ranged from 0.3 to 1.7 ms, corresponding to a temperature range from 1800 K to1300 K (considering the effect of temperature reduction due to probe insertion). The particle residence time (1.5 ms) was comparable to TTIP reaction time, indicating the measured clusters could be not fully reacted precursor clusters. The comparable time scales also suggested that the insertion of the cold dilution probe may affect the reaction of precursor molecules in the high temperature zone.

The performance of the dilution sampling system in quenching the particle growth dynamics can be evaluated through comparing the characteristic time scales of particle transport and particle coagulation in the sampling line. The transport time of particles can be calculated through dividing the volume of the transport line (tube with 4.35 mm diameter and 0.2 m length) by the gas flow rate (25 lpm), yielding a value of 7 ms. The characteristic coagulation time is dependent on the coagulation coefficient β and total particle concentration N_0, where

$$\tau_{coag} = \frac{2}{\beta N_0}. \tag{4}$$

The coagulation coefficient for neutral particles in the free molecular regime is given by

$$\beta = \left(\frac{3}{4\pi}\right)^{1/6}\left(\frac{6k_bT}{\rho_p}\right)^{1/2}\left(\frac{1}{v_i}+\frac{1}{v_j}\right)^{1/2}\left(v_i^{1/3}+v_j^{1/3}\right)^2, \tag{5}$$

where k_b is the Boltzmann constant, ρ_p is the particle density, T is temperature, and v_i is the volume of the particle *i*. Based on this equation, the self-coagulation coefficient of 1 to 2 nm particles ranges from 1.0×10^{-16} to 1.4×10^{-16} m^3/s at a temperature of 298 K . Further by assuming each TTIP molecule converted to a particle, the highest particle concentration (N_0) in the dilution probe after dilution was 1.7×10^{17} $/m^3$ (in the case of 0.22 mmol/hr, 8.8 ppm). The minimum characteristic coagulation time of incipient particles (τ_{coag}) was 84 ms, which was longer than the transport time of 7 ms. This comparison of time scales demonstrates that particle growth dynamics was sufficiently quenched in the dilution sampling system.

However, the suppression of gas-phase reactions could not be verified through similar calculations or experimental techniques, since critical information is missing on the reaction kinetics of incipient particles. Dilution sampling involves the reduction of temperature, which inevitably alters the equilibrium of reactions in the sampled stream. This influence may be substantial for the incipient particles that are physically and chemically instable. Due to the lower stability of nitrate species at elevated temperatures, the detected nitrate-bounded Ti-containing clusters might be formed through a post oxidation step during dilution, or between the sampling nozzle and the APi-TOF inlet. Furthermore, charged species typically observed in methane flames, for example, CH*, CHO^+, and $C_3H_3^+$, were not detected by the APi-TOF, implying the possible conversion of these species in the dilution system. It was possible that this conversion took place instantaneously, where increasing dilution ratio could not efficiently suppress the regarding chemical reactions. The chemical composition of the diluent gas (N_2) may also play a role in this rapid conversion of incipient particles. However, the research

findings of this study can still be applied in quantum dot synthesis and material molecular doping, where rapid dilution is needed to control the small size and uniform composition of particles. Future work can focus on the design, testing, and evaluation of dilution sampling systems for incipient particle measurement at high temperatures with various diluent gas species to ensure the validity of incipient particle measurements.

4. Conclusions

Through the measurement of natively charged clusters during the combustion synthesis of TiO_2, the clustering interactions between intermediate species of TTIP decomposition in a methane-air flat flame towards the formation of TiO_2 nanoparticles was studied. Measurements were made using an atmospheric pressure interface-time of flight mass spectrometer. Results show newly detected negatively charged species which include NO_x species attached to titanium species with different oxidation states and stable positive monomers of $Ti(OH)_4$ and $TiO(OH)_4$. Evidence from these measurements indicate the importance for intermediate clustering interactions which may be specific to precursor chemistry of flame condition. Through these series of measurements, we have observed several new phenomena: 1) The abstraction of CH_2 group dominates the mechanism of hydrocarbon removal in positively charged precursor clusters; 2) Intermediate organic species in the form of $Ti_nO_xC_yH_z$ may form lager complexes prior to complete conversion to TTIP; 3) $Ti(OH)_4$, $TiO(OH)_4$, and $TiO_2(NO_3)_3^-$ are the most stable monomeric Ti species that are natively charged; 4) Chemi-ionization can play a principle role in the initial stages of particle formation.

Acknowledgements:

This work is supported by the Solar Energy Research Institute for India and the United States (SERIIUS), funded jointly by the U.S. Department of Energy (Office of Science, Office of Basic Energy Sciences, and Energy Efficiency and Renewable Energy, Solar Energy Technology Program, under Subcontract DE-AC36-08GO28308 to the National Renewable Energy Laboratory, Golden, Colorado) and the Government of India, through the Department of Science and Technology under Subcontract IUSSTF/JCERDC-SERIIUS/2012. The work was also supported by Academy of Finland via Center of Excellence project in Atmospheric Sciences (272041) and European Commission via ACTRIS2 (654109).

References

Ahn, K.-H., Park, Y.-B., Park, D.-W. (2003). Kinetic and mechanistic study on the chemical vapor deposition of titanium dioxide thin films by in situ FTIR using TTIP. Surf. Coat. Technol. 171:198-204.

Biswas, P., Wu, C. Y., Zachariah, M. R., McMillin, B. (1997). Characterization of iron oxide-silica nanocomposites in flames .2. Comparison of discrete-sectional model predictions to experimental data. J. Mater. Res. 12:714-723.

Buerger, P., Nurkowski, D., Akroyd, J., Mosbach, S., Kraft, M. (2015). First-principles thermochemistry for the thermal decomposition of titanium tetraisopropoxide. J. Phys. Chem. A 119:8376-8387.

Buerger, P., Nurkowski, D., Akroyd, J., Kraft, M. (2017). A kinetic mechanism for the thermal decomposition of titanium tetraisopropoxide. Proc. Combust. Inst. 36:1019-1027.

Debrou, G. B., Goodings, J. M., Bohme, D. K. (1980). Flame-ion Probe Intermediates Leading to NOx in CH4- O2- N2 Flames. Combust. Flame 39:1-19.

Fang, J. X., Wang, Y., Attoui, M., Chadha, T. S., Ray, J. R., Wang, W. N., Jun, Y. S., Biswas, P. (2014). Measurement of Sub-2 nm Clusters of Pristine and Composite Metal Oxides during Nanomaterial Synthesis in Flame Aerosol Reactors. Anal. Chem. 86:7523-7529.

Fialkov, A. B. (1997). Investigations on ions in flames. Prog. Energy Combust. Sci. 23:399-528.

Guan, B., Lu, W., Fang, J., Cole, R. B. (2007). Characterization of synthesized titanium oxide nanoclusters by MALDI-TOF mass spectrometry. J. Am. Soc. Mass. Spectrom. 18:517-524.

Hansen, N., Cool, T. A., Westmoreland, P. R., Kohse-Höinghaus, K. (2009). Recent contributions of flame-sampling molecular-beam mass spectrometry to a fundamental understanding of combustion chemistry. Prog. Energy Combust. Sci. 35:168-191.

Hu, Y., Jiang, H., Li, Y., Wang, B., Zhang, L., Li, C., Wang, Y., Cohen, T., Jiang, Y., Biswas, P. (2016). Engineering the outermost layers of TiO_2 nanoparticles using in situ Mg doping in a flame aerosol reactor. AIChE J.

Hughey, C. A., Hendrickson, C. L., Rodgers, R. P., Marshall, A. G., Qian, K. (2001). Kendrick mass defect spectrum: a compact visual analysis for ultrahigh-resolution broadband mass spectra. Anal. Chem. 73:4676-4681.

Jiang, J., Lee, M.-H., Biswas, P. (2007). Model for nanoparticle charging by diffusion, direct photoionization, and thermionization mechanisms. J. Electrostat. 65:209-220.

Jones, H. R. and Hayhurst, A. N. (2016). Measurements of the concentrations of positive and negative ions along premixed fuel-rich flames of methane and oxygen. Combust. Flame 166:86-97.

Junninen, H., Ehn, M., Petäjä, T., Luosujärvi, L., Kotiaho, T., Kostiainen, R., Rohner, U., Gonin, M., Fuhrer, K., Kulmala, M. (2010). A high-resolution mass spectrometer to measure atmospheric ion composition. Atmos. Meas. Tech. 3:1039-1053.

Kluge, S., Wiggers, H., Schulz, C. (2016). Mass spectrometric analysis of clusters and nanoparticles during the gas-phase synthesis of tungsten oxide. Proc. Combust. Inst.

Kulmala, M., Kontkanen, J., Junninen, H., Lehtipalo, K., Manninen, H. E., Nieminen, T., Petäjä, T., Sipilä, M., Schobesberger, S., Rantala, P. (2013). Direct observations of atmospheric aerosol nucleation. Science 339:943-946.

Larriba, C. and Hogan Jr, C. J. (2013). Ion mobilities in diatomic gases: measurement versus prediction with non-specular scattering models. J. Phys. Chem. A 117:3887-3901.

Larriba, C., Hogan Jr, C. J., Attoui, M., Borrajo, R., Garcia, J. F., de la Mora, J. F. (2011). The mobility–volume relationship below 3.0 nm examined by tandem mobility–mass measurement. Aerosol Sci. Technol. 45:453-467.

Li, S., Ren, Y., Biswas, P., Stephen, D. T. (2016). Flame aerosol synthesis of nanostructured materials and functional devices: Processing, modeling, and diagnostics. Prog. Energy Combust. Sci. 55:1-59.

Liu, P., Arnold, I. J., Wang, Y., Yu, Y., Fang, J., Biswas, P., Chakrabarty, R. K. (2015). Synthesis of titanium dioxide aerosol gels in a buoyancy-opposed flame reactor. Aerosol Sci. Technol. 49:1232-1241.

Liu, C., Li, S., Zong, Y., Yao, Q., Stephen, D. T. (2016). Laser-based investigation of the transition from droplets to nanoparticles in flame-assisted spray synthesis of functional nanoparticles. Proc. Combust. Inst.

McMillin, B. K., Biswas, P., Zachariah, M. R. (1996). In situ characterization of vapor phase growth of iron oxide-silica nanocomposites .1. 2-D planar laser-induced fluorescence and Mie imaging. J. Mater. Res. 11:1552-1561.

Nicol, D. G., Steele, R. C., Marinov, N. M., Malte, P. C. (1995). The importance of the nitrous oxide pathway to NOx in lean-premixed combustion. J. Eng. Gas Turbines Power 117:100-111.

Nie, Y., Wang, Y., Biswas, P. (2017). Mobility and bipolar diffusion charging characteristics of crumpled reduced graphene oxide nanoparticles synthesized in a furnace aerosol reactor. *J. Phys. Chem. C.* doi: 10.1021/acs.jpcc.7b00189.

Okuyama, K., Ushio, R., Kousaka, Y., Flagan, R. C., Seinfeld, J. H. (1990). Particle generation in a chemical vapor deposition process with seed particles. AIChE J. 36:409-419.

Park, D. G., Chung, S. H., Cha, M. S. (2016). Bidirectional ionic wind in nonpremixed counterflow flames with DC electric fields. Combust. Flame 168:138-146.

Pratsinis, S. E. (1998). Flame aerosol synthesis of ceramic powders. Prog. Energy Combust. Sci. 24:197-219.

Ren, Y., Zhang, Y., Li, S., Law, C. K. (2015). Doping mechanism of Vanadia/Titania nanoparticles in flame synthesis by a novel optical spectroscopy technique. Proc. Combust. Inst. 35:2283-2289.

Ren, Y., Li, S., Cui, W., Zhang, Y., Ma, L. (2017). Low-frequency AC electric field induced thermoacoustic oscillation of a premixed stagnation flame. Combust. Flame 176:479-488.

Schobesberger, S., Junninen, H., Bianchi, F., Lönn, G., Ehn, M., Lehtipalo, K., Dommen, J., Ehrhart, S., Ortega, I. K., Franchin, A. (2013). Molecular understanding of atmospheric particle formation from sulfuric acid and large oxidized organic molecules. PNAS 110:17223-17228.

Shmakov, A. G., Korobeinichev, O. P., Knyazkov, D. A., Paletsky, A. A., Maksutov, R. A., Gerasimov, I. E., Bolshova, T. A., Kiselev, V. G., Gritsan, N. P. (2013). Combustion chemistry of $Ti(OC_3H_7)_4$ in premixed flat burner-stabilized H_2/O_2/Ar flame at 1 atm. Proc. Combust. Inst. 34:1143-1149.

Siefering, K. and Griffin, G. (1990). Growth kinetics of CVD TiO_2: influence of carrier gas. J. Electrochem. Soc. 137:1206-1208.

Swihart, M. T. (2003). Vapor-phase synthesis of nanoparticles. Curr. Opin. Colloid Interface Sci. 8:127-133.

Tsantilis, S., Kammler, H., Pratsinis, S. (2002). Population balance modeling of flame synthesis of titania nanoparticles. Chem. Eng. Sci. 57:2139-2156.

Ulrich, G. D. (1971). Theory of particle formation and growth in oxide synthesis flames. Combust. Sci. Technol. 4:47-57.

Wang, Y., Fang, J., Attoui, M., Chadha, T. S., Wang, W.-N., Biswas, P. (2014). Application of Half Mini DMA for sub 2 nm particle size distribution measurement in an electrospray and a flame aerosol reactor. J. Aerosol Sci. 71:52-64.

Wang, Y., Kangasluoma, J., Attoui, M., Fang, J., Junninen, H., Kulmala, M., Petäjä, T., Biswas, P. (2017a). Observation of incipient particle formation during flame synthesis by tandem differential mobility analysis-mass spectrometry (DMA-MS). Proc. Combust. Inst. just accepted.

Wang, Y., Kangasluoma, J., Attoui, M., Fang, J., Junninen, H., Kulmala, M., Petäjä, T., Biswas, P. (2017b). The high charge fraction of flame-generated particles in the size range below 3 nm measured by enhanced particle detectors. Combust. Flame 176:72-80.

Wang, Y., Liu, P., Fang, J., Wang, W.-N., Biswas, P. (2015). Kinetics of sub-2 nm TiO_2 particle formation in an aerosol reactor during thermal decomposition of titanium tetraisopropoxide. J. Nanopart. Res. 17:1-13.

Wang, Y., Sharma, G., Koh, C., Kumar, V., Chakrabarty, R. K., Biswas, P. (2017c). Influence of flame-generated ions on the simultaneous charging and coagulation of nanoparticles during combustion. Aerosol Sci. Technol. doi: 10.1080/02786826.2017.1304635.

Xiong, G., Kulkarni, A., Dong, Z., Li, S., Stephen, D. T. (2017a). Electric-field-assisted stagnation-swirl-flame synthesis of porous nanostructured titanium-dioxide films. Proc. Combust. Inst. 36:1065-1075.

Xiong, Y., Chung, S. H., Cha, M. S. (2017b). Instability and electrical response of small laminar coflow diffusion flames under AC electric fields: Toroidal vortex formation and oscillating and spinning flames. Proc. Combust. Inst. 36:1621-1628.

Zhang, Y. Y., Xiong, G., Li, S. Q., Dong, Z. Z., Buckley, S. G., Tse, S. D. (2013). Novel low-intensity phase-selective laser-induced breakdown spectroscopy of TiO_2 nanoparticle aerosols during flame synthesis. Combust. Flame 160:725-733.

Zhao, B., Yang, Z., Wang, J., Johnston, M. V., Wang, H. (2003). Analysis of soot nanoparticles in a laminar premixed ethylene flame by scanning mobility particle sizer. Aerosol Sci. Technol. 37:611-620.

TABLE CAPTIONS

Table 1: Characteristics of the methane-air flat flame aerosol reactor

Table 2: Experimental plan for measuring cluster formation pathways

Table 3: Proposed molecular compositions for identified peaks in a negative mass spectrum

FIGURE CAPTIONS

FIG. 1. Experimental setup of the flat flame aerosol reactor for measurement of natively charged clusters in an atmospheric pressure interface time-of-flight mass spectrometer.

FIG. 2. Background ions measured in a flame aerosol reactor for naturally charged positive (left) and negative (right) ions, with nominal masses of major peaks labeled. For negatively charged flame clusters, larger peaks beyond 100 Th were scaled by multiplying the signal intensity by 20 (20X).

FIG. 3. Negative TTIP spectra at two different precursor feed rates of 0.07 mmol/hr (top) and 0.15 mmol/hr (bottom). Colored spectra refer to portions of the mass spectra where signal intensities were scaled by a factor of 2 (2X), 5 (5X) and 10 (10X).

FIG. 4. Positively charged clusters during the combustion synthesis of TiO_2 at three different feed rates of 0.07, 0.15, and 0.22 mmol/hr.

FIG. 5. Mass defect plots for positively charged clusters (a) and negatively charged clusters (b) during the combustion synthesis of TiO_2.

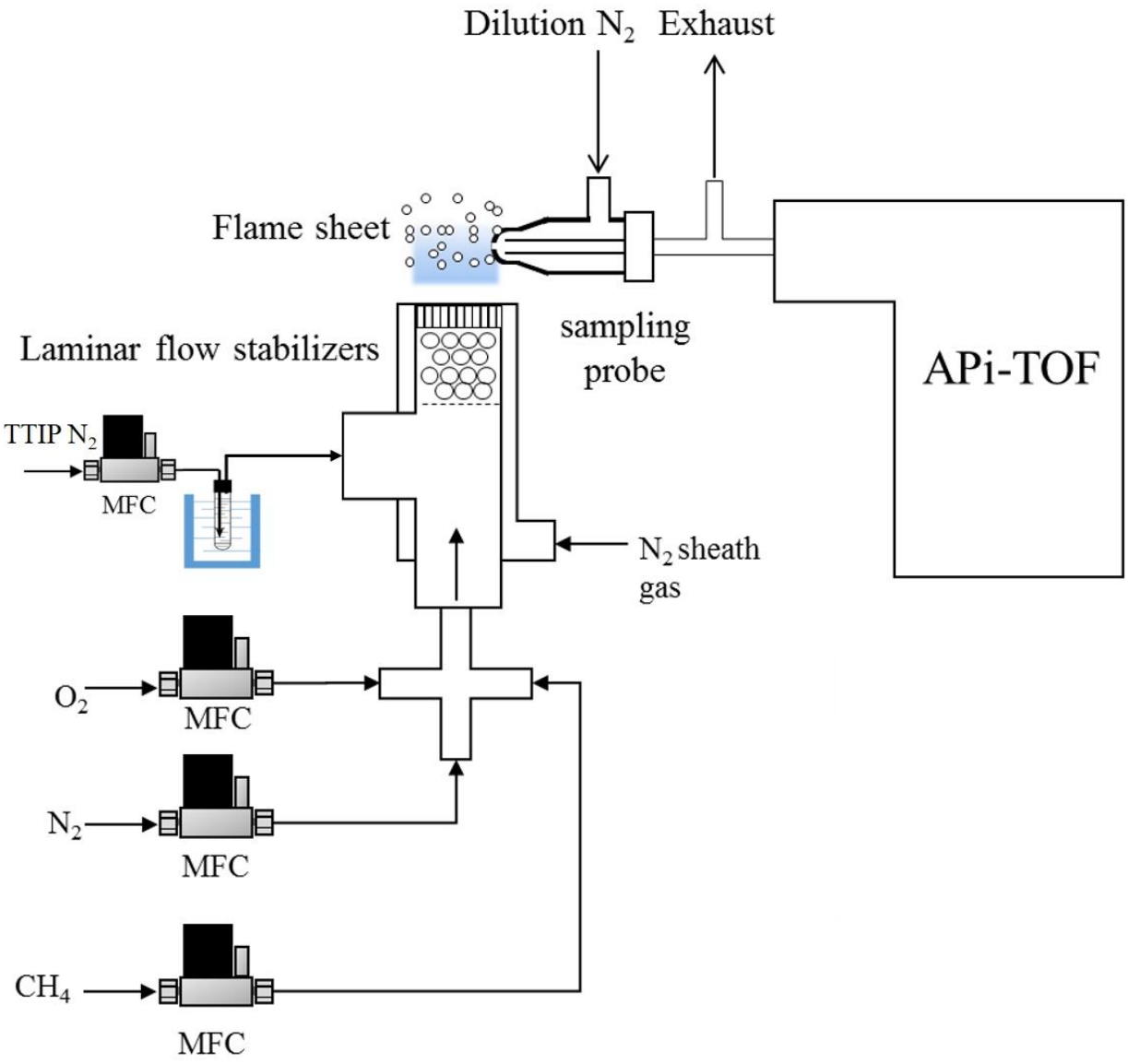

Figure 1: Experimental setup of the flat flame aerosol reactor for measurement of natively charged clusters in an atmospheric pressure interface time-of-flight mass spectrometer.

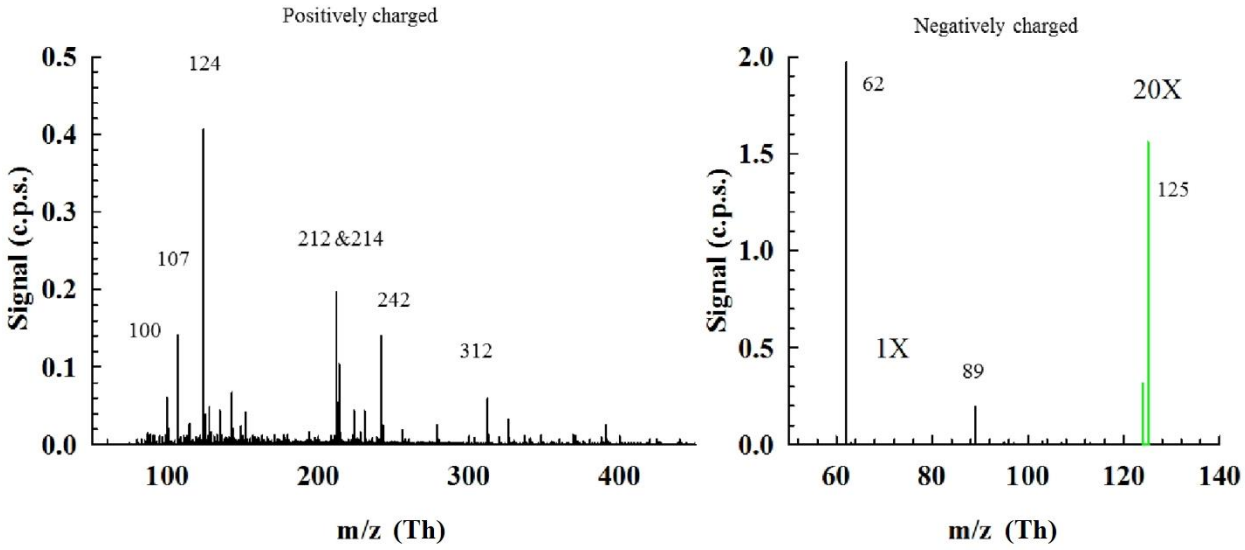

Figure 2: Background ions measured in a flame aerosol reactor for naturally charged positive (left) and negative (right) ions, with nominal masses of major peaks labeled. For negatively charged flame clusters, larger peaks beyond 100 Da were scaled by multiplying the signal intensity by 20 (20X).

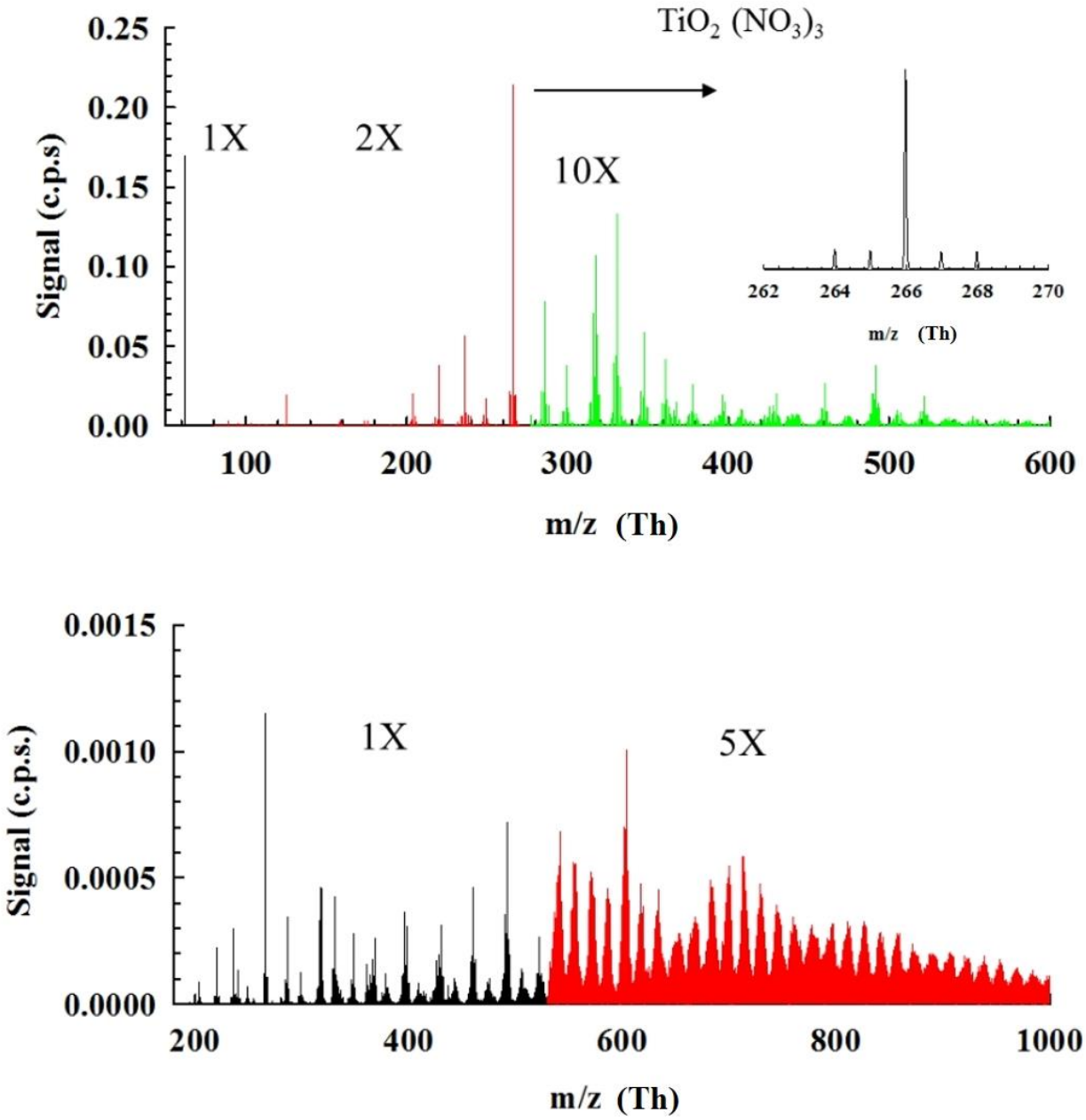

Figure 3: Negative TTIP spectra at two different precursor feed rates of 0.07 mmol/hr (top) and 0.15 mmol/hr (bottom). Colored spectra refer to portions of the mass spectra where signal intensities were scaled by a factor of 2 (2X), 5 (5X) and 10 (10X).

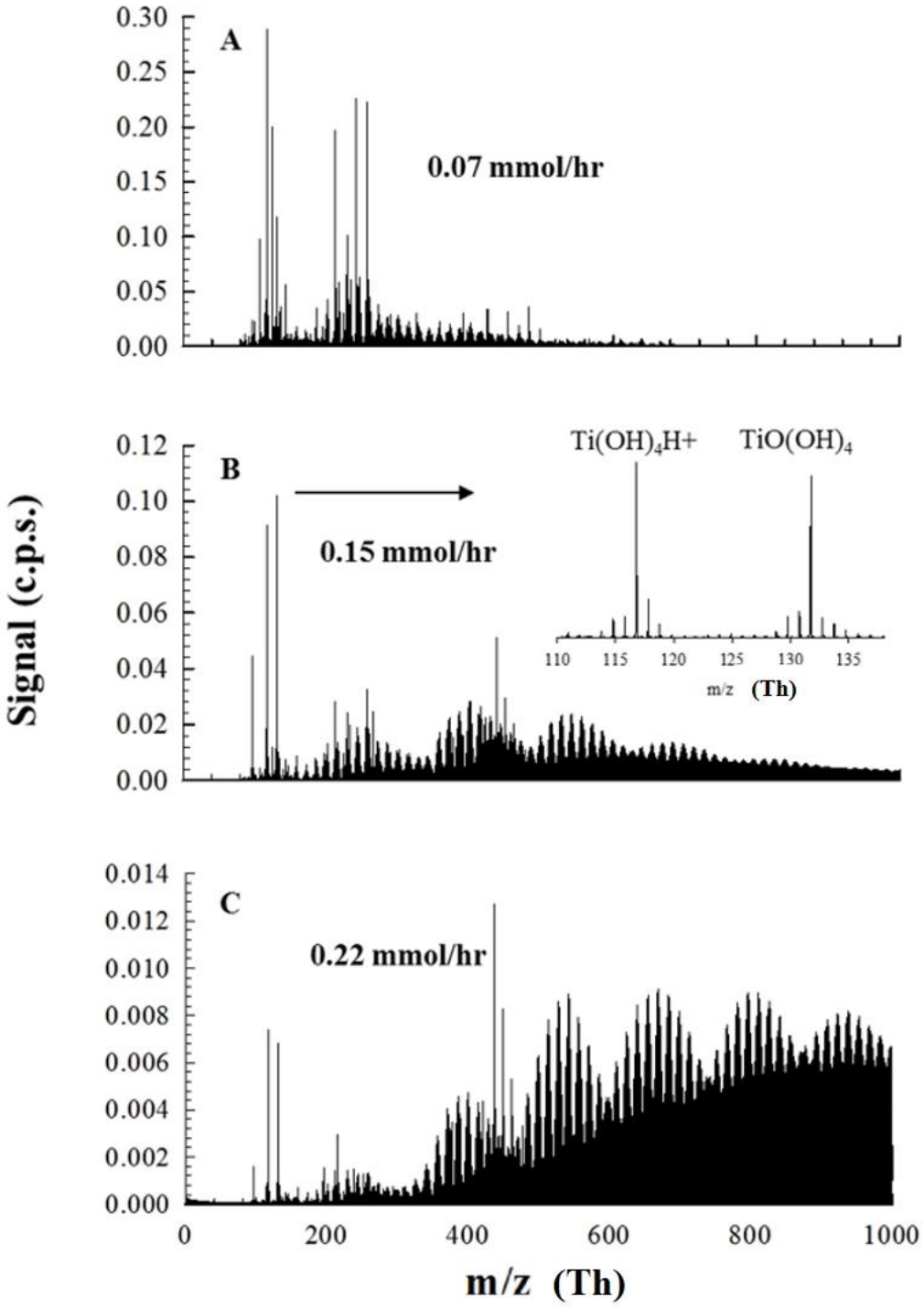

Figure 4: Positively charged clusters during the combustion synthesis of TiO_2 at three different loading rates of 0.07, 0.15, and 0.22 mmol/hr.

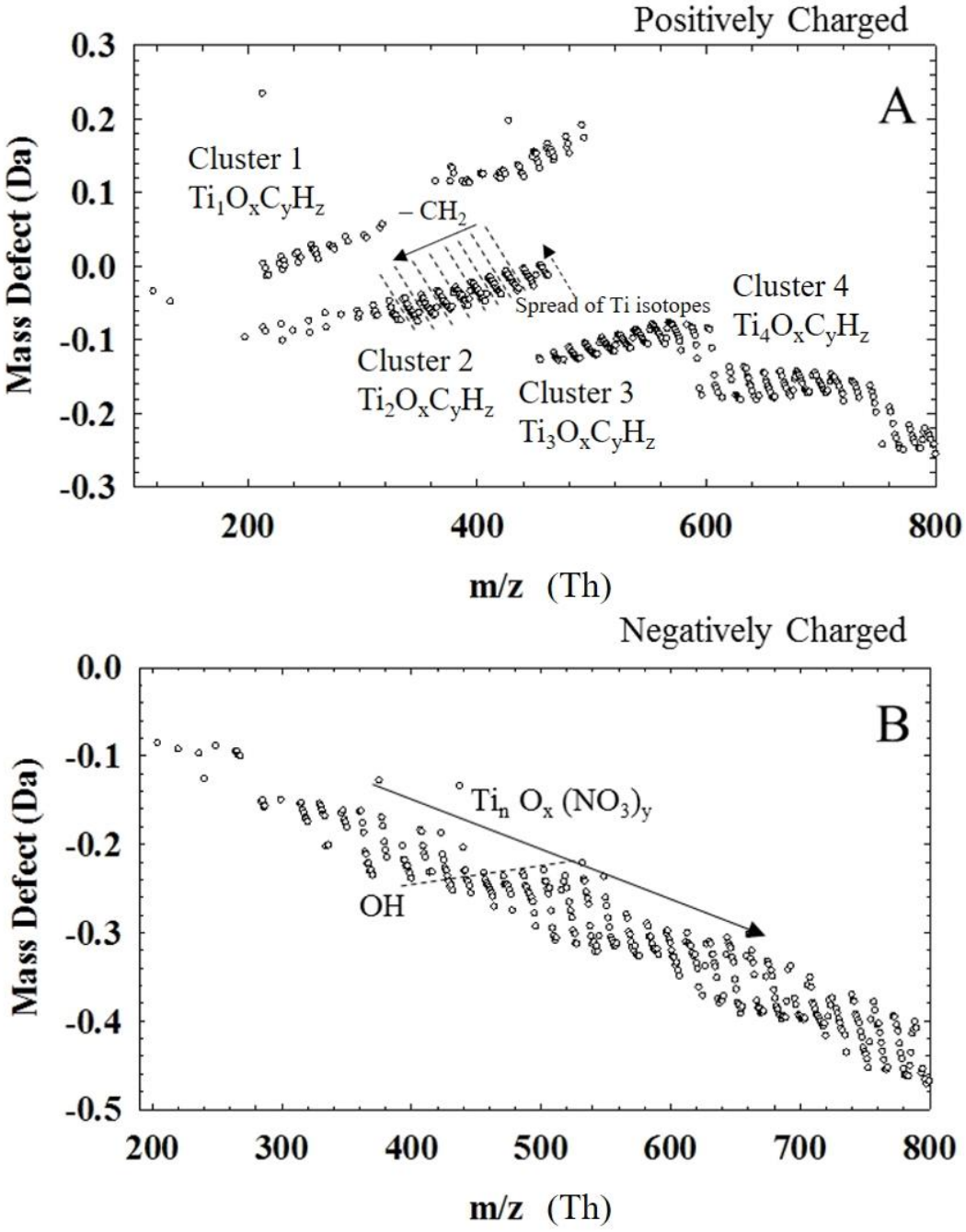

Figure 5: Mass defect plots for (a) positively charged ions and (b) negatively charged ions during the combustion synthesis of TiO_2.

Table 1: Characteristics of the methane-air flat flame aerosol reactor

Property	Value
CH_4flow rate	1.00 lpm
O_2 flow rate	2.85 lpm
N_2 flow rate	6.50 lpm
Sheath N_2 flow rate	3.00 lpm
Dilution ratio	180:1
Precursor feed rates	0.07 – 0.22 mmol/hr (2.8 – 8.8 ppm)
Flame diameter	1.91 cm

Table 2: Experimental plan for measuring cluster formation pathways

Test #	Objective
1	Background natively charged clusters in the flame
2	Positive ion mass spectra for TTIP
3	Negative ion mass spectra for TTIP
4	Effect of loading rate on resultant mass spectra

Table 3: Proposed molecular compositions for identified peaks in a negative mass spectrum

Negatively Charged Clusters

Molecular Formula	Exact Mass	Measured Mass	ppm
TiO_8N_2	203.9140	203.914	-1.67
TiO_9N_2	219.9089	219.908	3.78
$TiO_{10}N_2$	235.9038	235.903	3.31
$Ti_2O_8H_2N$	239.8745	239.873	2.45
$TiO_{11}N_3$	265.9012	265.901	0.88
$Ti_2O_{11}N$	285.8430	285.843	1.89
$Ti_2O_{11}CHN$	298.8509	298.851	-1.14
$Ti_2O_{12}N_2$	315.8410	315.838	10.60
$Ti_2O_{13}N$	317.8329	317.830	9.12
$Ti_3O_9C_2H_5N$	330.8403	330.838	6.95
$Ti_3O_{11}H_4C_2$	347.8192	347.819	9.28